BIOCHEMISTRY
including biophysical chemistry & molecular biology
Article

Biochemistry **2009,** *48,* 6423–6430 6423
DOI: 10.1021/bi900590m

Role of the Sulfonium Center in Determining the Ligand Specificity of Human *S*-Adenosylmethionine Decarboxylase[†,‡]

Shridhar Bale,[§] Wesley Brooks,[∥] Jeremiah W. Hanes,[§] Arnold M. Mahesan,[§] Wayne C. Guida,[∥,⊥] and Steven E. Ealick*[,§]

[§]*Department of Chemistry and Chemical Biology, Cornell University, Ithaca, New York 14853,* [∥]*Drug Discovery Program, H. Lee Moffitt Cancer Center and Research Institute, Tampa, Florida 33612, and* [⊥]*Departments of Chemistry and Oncologic Sciences, University of South Florida, Tampa, Florida 33620*

Received April 6, 2009; Revised Manuscript Received May 18, 2009

ABSTRACT: *S*-Adenosylmethionine decarboxylase (AdoMetDC) is a key enzyme in the polyamine biosynthetic pathway. Inhibition of this pathway and subsequent depletion of polyamine levels is a viable strategy for cancer chemotherapy and for the treatment of parasitic diseases. Substrate analogue inhibitors display an absolute requirement for a positive charge at the position equivalent to the sulfonium of *S*-adenosylmethionine. We investigated the ligand specificity of AdoMetDC through crystallography, quantum chemical calculations, and stopped-flow experiments. We determined crystal structures of the enzyme cocrystallized with 5′-deoxy-5′-dimethylthioadenosine and 5′-deoxy-5′-(*N*-dimethyl)amino-8-methyladenosine. The crystal structures revealed a favorable cation−π interaction between the ligand and the aromatic side chains of Phe7 and Phe223. The estimated stabilization from this interaction is 4.5 kcal/mol as determined by quantum chemical calculations. Stopped-flow kinetic experiments showed that the rate of the substrate binding to the enzyme greatly depends on Phe7 and Phe223, thus supporting the importance of the cation−π interaction.

The polyamines putrescine, spermidine, and spermine are aliphatic polycations that are critical for maintaining cell differentiation and proliferation (*1*−*3*). Elevated levels of polyamines are found in cancerous and tumor cell lines (*4*, *5*). Thus, depleting polyamine levels by inhibition of the polyamine biosynthetic pathway is a promising approach for the treatment and prevention of cancer and also for the treatment of various parasitic diseases. *S*-Adenosylmethionine decarboxylase (AdoMetDC)[1] is a key enzyme in the polyamine biosynthetic pathway and depends on a pyruvoyl cofactor for the decarboxylation reaction (*6*−*9*). AdoMetDC catalyzes the decarboxylation of *S*-adenosylmethionine (AdoMet) to *S*-adenosyl-5′-(3-methylthiopropylamine) (dcAdoMet). The aminopropyl group from dcAdoMet is transferred to putrescine or spermidine to form spermidine or spermine, respectively. AdoMetDC catalyzes an early step in the pathway, and dcAdoMet is completely committed to polyamine biosynthesis; thus, AdoMetDC is an attractive target for drug design.

The early inhibitors of AdoMetDC included the potent competitive inhibitor methylglyoxal bis(guanylhydrazone) (MGBG) (*10*). Clinical studies on this compound were hampered by an unexpected mitochondrial toxicity unrelated to its inhibition of AdoMetDC. An MGBG analogue, 4-amidinoindan-1-one-2′-amidinohydrazone (CGP48664A), showed promise in multiple phase I and phase II clinical trials (*11*−*18*). Irreversible (or slowly reversible) substrate analogue inhibitors, which form a Schiff base with the active site pyruvoyl group, have also been synthesized but are limited by their nonspecific activity toward cellular aldehydes and ketones (*19*). In vitro assays showed that a positive charge at the position of the sulfonium ion substrate analogues is essential for ligand binding and inhibition (*20*). Thioether and sulfoxide substrate analogues, which lack the positive charge, exhibited no activity. On the other hand, replacement of a sulfur atom with a nitrogen atom, which is protonated at physiological pH and retains the positive charge, resulted in AdoMetDC inhibition. This is consistent with the observation that *S*-adenosylhomocysteine (SAH) is not a substrate for AdoMetDC (*21*).

[†]This work was supported by National Cancer Institute Grant CA-094000 (to S.E.E.) from the National Institutes of Health. S.E.E. is also indebted to the W. M. Keck Foundation and the Lucille P. Markey Charitable Trust.

[‡]The Protein Data Bank entries for the complexes are as follows: 3H0V for AdoMetDC and MMTA and 3H0W for AdoMetDC and DMAMA.

*To whom correspondence should be addressed: Department of Chemistry and Chemical Biology, Cornell University, Ithaca, NY 14853. Telephone: (607) 255-7961. Fax: (607) 255-1227. E-mail: see3@cornell.edu.

[1]Abbreviations: AdoMetDC, *S*-adenosylmethionine decarboxylase; AdoMet, *S*-adenosylmethionine; MeAdoMet, *S*-adenosylmethionine methyl ester; dcAdoMet, *S*-adenosyl-5′-(3-methylthiopropylamine); SAH, *S*-adenosylhomocysteine; MMTA, 5′-deoxy-5′-(dimethylsulfonio)adenosine; MTA, 5′-deoxy-5′-methylthioadenosine; DMAMA, 5′-deoxy-5′-(*N*-dimethyl)amino-8-methyladenosine; MGBG, methylglyoxal bis(guanylhydrazone); CGP48664A, 4-amidinoindan-1-one-2′-amidinohydrazone; MAOEA, 5′-deoxy-5′-{*N*-methyl-*N*-[(2-aminooxy)ethyl]amino}adenosine; MHZPA, 5′-deoxy-5′-[*N*-methyl-*N*-(3-hydrazinopropyl)amino]adenosine; WT, wild type; HEPES, *N*-(2-hydroxyethyl)piperazine-*N*′-2-ethanesulfonic acid; DTT, dithiothreitol; Brij-35, polyoxyethylene glycol dodecyl ether; HF, Hartree−Fock; LMP2, local Moller−Plesset second-order perturbation; SCRF, self-consistent reaction field.

Published on Web 06/15/2009

Previously, the structures of AdoMetDC and its complexes with inhibitors 5′-deoxy-5′-[*N*-methyl-*N*-(3-hydrazinopropyl) amino]adenosine (MHZPA), 5′-deoxy-5′-{*N*-methyl-*N*-[(2-aminooxy)ethyl]amino}adenosine (MAOEA), the methyl ester of AdoMet (MeAdoMet), MGBG, and CGP48664A were determined (*22*). MGBG and CGP48664A act as competitive inhibitors of the enzyme and stack between Phe7 and Phe223 and form hydrogen bonds with Glu247, Ser229, and the backbone amide of Leu65. The substrate analogues MHZPA, MAOEA, and MeAdoMet have positive charges at the sulfonium ion position and covalently bind to the enzyme acting as slowly reversible inhibitors. The adenine base of these inhibitors stacks between Phe7 and Phe223; the glycosidic bond adopts an unusual *syn* conformation, and both ribose hydroxyl groups hydrogen bond to Glu247. The requirement for a positive charge in substrate analogues remained puzzling because no negatively charged amino acid side chain was located nearby.

We chose to investigate the basis of the ligand specificity of AdoMetDC using crystallography, quantum chemical calculations, and stopped-flow kinetic experiments. We determined crystal structures of the enzyme cocrystallized with 5′-deoxy-5′-(dimethylsulfonio)adenosine (MMTA) and 5′-deoxy-5′-(*N*-dimethyl)amino-8-methyladenosine (DMAMA). The energy difference between the *syn* and *anti* conformations of the ligands in solution and in the active site of the enzyme was obtained using quantum chemical calculations. Stopped-flow kinetic experiments were conducted to investigate the importance of Phe7 and Phe223, two residues located near the positive charge. Our results show that ligand specificity in human AdoMetDC is mainly due to cation$-\pi$ interactions and to electrostatic interactions between N3 of adenine and the sulfonium ion, which stabilizes the *syn* conformation.

MATERIALS AND METHODS

Materials. The syntheses of MMTA and DMAMA were previously reported (*23*), and the compounds were gifts from J. Secrist at Southern Research Institute (Birmingham, AL).

Protein Expression and Purification. The gene encoding AdoMetDC was cloned into a pQE30 vector and transformed into JM109 *Escherichia coli* cells. Cells were grown in LB medium supplemented with 100 mg/mL ampicillin at 37 °C until the absorbance reached an OD_{600} of 0.6, at which point the cells were induced with 100 mg/L isopropyl 1-β-D-galactopyranoside, and the temperature was reduced to 15 °C. The cells were allowed to grow overnight before being harvested by centrifugation, washed using a lysis buffer containing 20 mM Na_2HPO_4 (pH 7.0), 500 mM NaCl, 2.5 mM putrescine, 0.02% polyoxyethylene glycol dodecyl ether (Brij-35), and 10 mM imidazole, and stored at −80 °C. The frozen cell pellet was resuspended in lysis buffer and lysed using a French press at 1500 psi. The cellular debris was separated from the lysate by centrifugation at 12000*g*. The cell lysate was incubated with Talon metal affinity resin for 1.5 h. The protein−resin complex was packed into a column and washed with 15−20 column volumes of wash buffer, which is the lysis buffer supplemented with 25 mM imidazole. The protein was eluted with the wash buffer containing 200 mM imidazole. The elute was further purified through a Superdex 75 column using a buffer containing 10 mM *N*-(2-hydroxyethyl)piperazine-*N*′-2-ethanesulfonic acid (HEPES) (pH 7.5), 2.5 mM putrescine, 5 mM DTT, 0.1 mM ethylenediaminetetraacetic acid (EDTA), 0.02% Brij-35, and 300 mM NaCl. The fractions containing the protein were pooled, concentrated to 10 mg/mL, and stored at −80 °C. The construction, expression, and purification of the mutants were described previously (*22*, *23*).

Crystallization. The protein was buffer exchanged into 10 mM HEPES (pH 7.5), 200 mM NaCl, and 1 mM DTT using Bio-Rad buffer exchange chromatography columns. The protein was incubated separately with a 4−6-fold molar excess of MMTA and DMAMA for 24 h prior to crystallization. The crystals were grown using the hanging drop method at 22 °C in 13−16% polyethylene glycol 8000, 100 mM tris(hydroxymethyl) aminomethane (pH 8.0−9.0), and 10 mM DTT. Crystals appeared overnight and were stable for 1−2 weeks but deteriorated thereafter.

Data Collection and Processing. The crystals were sequentially transferred to solutions containing the well solution with 2, 5, 8, 15, and 18% glycerol with equilibration for 1−2 min between each step. The crystals were flash-frozen under liquid nitrogen before being placed in the liquid nitrogen stream. The data for the complex of AdoMetDC with MMTA were collected at NE-CAT beamline 8-BM at the Advanced Photon Source using an ADSC Quantum 315 detector (Area Detector Systems Corp.). Data were collected over a rotation range of 200° with an oscillation range of 1° and a 60 s exposure per frame with a detector to crystal distance of 320 mm. The data for the complex of DMAMA were collected on NE-CAT beamline 24-ID-C. Data were collected over a rotation range of 200° with an oscillation range of 1° and 1 s exposure per frame with a detector to crystal distance of 250 mm. The data for the complexes were indexed, integrated, and scaled using the HKL2000 program suite (*24*). The data collection statistics for both complexes are summarized in Table 1.

Structure Determination and Refinement. The structures of the complexes were determined by molecular replacement with CNS (*25*) using the structure of the AdoMetDC−MeAdoMet complex [Protein Data Bank (PDB) entry 1i7B] as the search model. Model building for the complex of MMTA was performed using O (*26*). The model building for the complex of DMAMA was performed using Coot (*27*). The initial model obtained from molecular replacement was adjusted using composite omit maps and refined using successive rounds of simulated annealing, minimization, *B*-factor refinement, generation of new composite omit maps, difference Fourier maps, and model building. After a few rounds of refinement, the positions and conformations of the ligand molecules were identified using the improved difference Fourier maps and composite omit maps. The ligands were included in the models, and water molecules were added on the basis of the peaks in the difference Fourier maps. The parameter and the topology files for the ligands were generated using the HIC-Up server (*28*). The difference maps also showed density for a molecule of putrescine bound in each of the structures. The final refinement statistics for both complexes are given in Table 2.

Quantum Mechanical Calculations. The quantum chemical calculations on the cation$-\pi$ interactions were performed using Jaguar version 6.0 or 6.5 (Schrödinger). The X-ray structure of MMTA bound to AdoMetDC was employed for these calculations, and single-point energy calculations were performed using the LMP2/6-31G** method on the following: $(CH_3)_3S^+$ (from MMTA) plus two benzene rings (from Phe7 and Phe223), $(CH_3)_3S^+$ (from MMTA) plus one benzene ring (from Phe223), $(CH_3)_3S^+$ (from MMTA) plus one benzene ring (from Phe7), $(CH_3)_3S^+$ alone, benzene alone, $(CH_3)_2S$ (from MMTA)

Table 1: Data Collection Statistics for AdoMetDC Complexes

	AdoMetDC−MMTA	AdoMetDC−DMAMA
wavelength (Å)	0.9795	0.9795
space group	*C*2	*C*2
a (Å)	93.85	99.45
b (Å)	49.54	50.02
c (Å)	70.00	68.69
β (deg)	105.03	105.32
resolution (Å)	2.24	1.81
total no. of reflections/no. of unique reflections	56742/15123	107489/29093
redundancy[a]	3.9 (4.0)	3.7 (2.5)
% complete[a]	95.1 (99.4)	95.8 (73.5)
I/σ[a]	8.9 (4.26)	17.7 (3.4)
R_{sym}[a,b]	10.5 (31.7)	7.9 (21.5)
Matthews number	2.05	2.19
solvent content (%)	38.9	42.9

[a] Values for the highest-resolution shell are given in parentheses. [b] $R_{sym} = \sum\sum_i|I_i - \langle I\rangle|/\sum\langle I\rangle$, where $\langle I\rangle$ is the mean intensity of the N reflections with intensities I_i and common indices h,k,l.

Table 2: Refinement Statistics for AdoMetDC Complexes

	AdoMetDC−MMTA	AdoMetDC−DMAMA
resolution (Å)	2.24	1.81
R-factor[a]	0.226	0.193
R_{free}[b]	0.274	0.218
no. of non-H atoms		
protein	2405	2439
ligand	21	22
water	76	234
B-factor (Å^2)		
protein	32.6	29.3
ligand	43.1	22.8
putrescine	35.0	47.7
root-mean-square deviation		
bonds (Å)	0.006	0.008
angles (deg)	1.3	1.3
dihedrals (deg)	25.1	25.3
Ramachandran plot (%)		
most favored region	90.7	92.0
additional favored region	8.5	6.9
generously allowed region	0.8	0.8
disallowed region	0.0	0.4

[a] *R*-factor $= \sum_{hkl}||F_{obs}| - k|F_{cal}||/\sum_{hkl}|F_{obs}|$, where F_{obs} and F_{cal} are observed and calculated structure factors, respectively. [b] For R_{free}, the sum is extended over a subset of reflections (5%) excluded from all stages of refinement.

plus two benzene rings (from Phe223 and Phe7), and $(CH_3)_2S$ alone. The level of theory for the calculations is sufficient to account for the polarization effect and hence cation−π interactions (*29*).

The energies and conformations of MMTA and 5′-deoxy-5′-methylthioadenosine (MTA) in solution were determined starting with the NMR structure of AdoMet in solution (*30*) and truncating the molecule to MMTA or MTA. The *syn* conformation was obtained by adjusting the O−C1′−N9−C4 torsion angle. The structures were subjected to geometry optimization using the B3LYP/6-31G* density functional method and the SCRF implicit aqueous solvation model available in Jaguar. The single-point energy of the geometry-optimized structures was then obtained using the local Moller−Plesset second-order perturbation (LMP2)/cc-PVTZ(-f) method with aqueous self-consistent reaction field (SCRF) solvation.

The energies of the *syn* and *anti* conformations of MMTA in complex with the enzyme were determined using the MMTA complex as the basis. The truncated model for the *syn* conformation consisted of MMTA and residues Phe223 and Phe7. Backbone atoms of the adjacent residues were also included in the calculations. In addition, an acetate moiety derived from Glu247 was included. Hydrogen atoms were added to the model. Constrained geometry optimization was performed at the Hartree−Fock (HF)/6-31G** level, and the single-point energy was then calculated at the LMP2//6-31G** level. All atoms were constrained during the geometry optimization except the adenine ring, the ribose C1′ atom, and the ribose hydroxyl groups. The *anti* conformation was generated from this truncated model by adjusting the O−C1′−N9−C4 torsion angle to −140° followed by geometry optimization as described above. The partial charges after geometry optimization were obtained for each atom.

Stopped-Flow Experiments. The stopped-flow experiments were performed using a KinTek Stopped-Flow apparatus (model SF-2004, KinTek Corp., Austin, TX). Experiments were conducted at 25 °C in 10 mM HEPES (pH 7.5), 200 mM NaCl, and 1 mM DTT. The time dependence of binding was measured by monitoring changes in the intrinsic protein fluorescence. An excitation wavelength of 298 nm (rather than the excitation maximum of ∼280 nm) was used to avoid problems associated with inner filtering caused by increasing the ligand concentration. Emission was observed using a band-pass filter centered at 340 nm (±10 nm). All reported concentrations refer to the final value after rapid mixing of the ligand with enzyme at a ratio of 1:1 (v/v). The final enzyme concentration was 25 μM for the WT protein and the F7A and E247A mutants and 100 μM for the F223A mutant. AdoMet was mixed with enzyme in an at least 4-fold excess to maintain pseudo-first-order conditions. Linear and nonlinear regression of the data were performed using GraFit 5 (Erithacus Software, Horley, Surrey, U.K.).

Figure Preparation. Structural figures were generated using PyMOL (*31*).

RESULTS

Cocrystallization of AdoMetDC with Ligands. The enzyme was cocrystallized in the presence of SAH, MMTA, DMAMA, and MTA. The crystallization experiments show that only MMTA and DMAMA bound to the enzyme in the crystal while MTA and SAH did not. Cocrystallization experiments with MTA and SAH were performed at increased concentrations and incubation times to increase the likelihood of binding at the active site; however, no active site density was observed.

Crystal Structure of AdoMetDC with MMTA. The overall fold of AdoMetDC is a four-layer $\alpha\beta\beta\alpha$ sandwich as previously described (*32*). AdoMetDC autoprocessing results in an α-subunit with an N-terminal pyruvoyl group and a smaller β-subunit (*32*, *33*). One molecule of putrescine is bound between the β-sheets for each monomer and is located ∼15−20 Å from the active site.

In the crystal structure of AdoMetDC with MMTA, loops containing residues 1−4, 22−26, 165−172, 288−299, and 328−334 were disordered and were excluded from the model. MMTA ribose forms hydrogen bonds to Glu247; the O2′−Oε2 distance is 3.2 Å, and the O3′−Oε1 distance is 2.7 Å. The sulfonium sulfur atom is 4.4 Å from the center of the Phe233 ring, and the closest contact of sulfur atom with Phe223 is 3.9 Å (Cε1). The methylene

carbon atom adjacent to the sulfonium ion of MMTA is 4.4 Å from the center of Phe7 and 3.6 Å from Cε2 of Phe7. The glycosidic bond of MMTA adopts a *syn* conformation, and the adenine ring stacks between Phe223 and Phe7. The stereoview of the electron density for MMTA in the active site is shown in Figure 1.

Crystal Structure of AdoMetDC with DMAMA. In the structure of AdoMetDC with DMAMA, the loops containing residues 1−3, 24−26, 165−173, 288−299, and 328−334 were missing in the crystal structure. The ribose makes two hydrogen bonds to Glu247 with the O2′−Oε2 distance being 2.9 Å and the O3′−Oε1 distance being 2.6 Å. The nitrogen is 4.7 Å from the center of Phe223 and 4.2 Å from Cε1 of Phe223. The methylene carbon atom adjacent to the nitrogen atom is 4.3 Å from the center of Phe7 and 3.7 Å from Cε2 of Phe7. The adenosine moiety of DMAMA is in a *syn* conformation with the adenine base stacking between Phe7 and Phe223. A stereoview of the electron density for DMAMA in the active site is shown in Figure 2.

Quantum Mechanical Calculations. The LMP2/6-31G** energies from the quantum mechanical calculations are listed in Table 3. The calculated gas phase binding energy of $(CH_3)_3S^+$ between two benzene rings in the same geometrical orientations as Phe7 and Phe223 is −5.09 kcal/mol. On the other hand, the binding energy of $(CH_3)_2S$ between two benzene rings in the same geometrical orientations as Phe7 and Phe223 is only −0.60 kcal/mol. These calculations suggest that the cation−π interaction provides an additional stabilization of approximately −4.5 kcal/mol. Similar calculations suggest that the energy for binding of $(CH_3)_3S^+$ to Phe223 is −3.15 kcal/mol and the energy for binding to Phe7 is −3.41 kcal/mol.

The ab inito energy of the *syn* conformation of MMTA in the complex with Phe223, Phe7, and Glu247 is −3039.28899965619 hartrees, and the energy of the *anti* conformation is −3039.26998403002 hartrees. Thus, the energy difference between the *syn* and *anti* conformations of MMTA in the active site is −11.93 kcal/mol, favoring the *syn* conformation. This would represent the stabilization of the *syn* conformation caused primarily by Phe223 and Phe7.

We also investigated the conformational energetics of MMTA and MTA in aqueous solution using quantum chemical calculations. The results are in agreement with the experimental results described by Markham et al. (*30*). These compounds prefer an *anti* conformation in aqueous solution. The LMP2/cc-PVTZ(-f)//B3LYP/6-31G* calculated energy difference between the *anti* and *syn* conformations was 1.06 kcal/mol for MMTA and 0.88 kcal/mol for MTA, favoring the *anti* conformation in each case.

Stopped-Flow Experiments. An intrinsic fluorescence change was observed when AdoMetDC was rapidly mixed with AdoMet. However, when SAH was mixed with AdoMetDC, there was no significant change other than that determined to be due to photobleaching (compared to a control without SAH). This indicates that SAH binding is much weaker and/or produces no discernible conformational change. The signal when MMTA was mixed with AdoMetDC was also too weak to measure the kinetics of the binding reaction.

Kinetic data for AdoMet binding to WT AdoMetDC along with the F223A, F7A, and E247A mutants were collected. For WT, F7A, and E247A, the data were best fit to a double-exponential equation

$$F = A_1 e^{-\lambda_1 t} + A_2 e^{-\lambda_2 t} + C$$

to yield the observed rates (λ_1 and λ_2) and amplitudes (A_1 and A_2) of the two phases at each concentration of AdoMet. The concentration dependencies of the fast and slow phases are plotted in Figure 3. The fast phase exhibited a linear concentration dependence and did not saturate. The slow phase was approximately hyperbolic and saturated at relatively low concentrations. The data are best described by a minimal model of two sequential steps:

$$E + S \underset{k_{-1}}{\overset{k_1}{\leftrightarrow}} EX \underset{k_{-2}}{\overset{k_2}{\leftrightarrow}} EA$$

According to this model, the fast phase of the reaction occurs at an observed rate approximately equal to the sum of all four intrinsic rate constants (*34*):

$$\lambda_1 \sim k_1[S] + k_{-1} + k_2 + k_{-2}$$

A linear fit of the fast phase (AdoMet binding to the WT enzyme) results in a k_1 of $0.136 \pm 0.005\ \mu M^{-1}\ s^{-1}$, a k_{-1} of $33 \pm 2\ s^{-1}$, and a $k_2 + k_{-2}$ value of $3.7 \pm 0.2\ s^{-1}$. Therefore, the dissociation constant (K_d) for binding of AdoMet to AdoMetDC can be estimated to be $242 \pm 17\ \mu M$ from the k_{-1}/k_1 ratio.

For the F7A and E247A mutants, the data were analyzed in a similar fashion except that a lower overall signal change caused photobleaching to become a significant component of the data. Therefore, the decrease due to photobleaching was corrected by using data from a control reaction mixture from which substrate had been omitted (resulting in a linear decrease in fluorescence). After correction, the kinetic parameters were obtained as for the WT enzyme. The values of k_{-1} and $k_2 + k_{-2}$ were similar for both mutants, but the value of the second-order rate constant for substrate binding (k_1) changed significantly. On the basis of the values of k_1 and k_{-1}, the K_d for the F7A mutant was $370 \pm 60\ \mu M$ and the K_d for the E247A mutant was 12.2 ± 3.6 mM.

The fluorescence change seen upon mixing AdoMet with the F223A mutant was best fit using a single-exponential equation. The concentration dependence of the observed rate varied linearly with a slope (k_1) of $(1.7 \pm 0.3) \times 10^{-4}\ \mu M^{-1}\ s^{-1}$ and a y-intercept (k_{-1}) of $2.4 \pm 0.2\ s^{-1}$, yielding a K_d of 14 ± 3 mM. Generally, the values measured here follow the same trend as the steady state kinetic parameters (k_{cat} and K_m) obtained previously (*22*). A comparison of K_d values for AdoMet binding to WT, F223A, F7A, and E247A reveals that the importance of residues for substrate binding decreases in the following order: F223A ∼ E247A ≫ F7A > WT.

DISCUSSION

Cation−π Interactions and Ligand Specificity of AdoMetDC. Cation−π interactions are ubiquitous in nature and aid in protein stability, ligand recognition, catalysis, and ion channel function (*35*, *36*). In the gas phase, the energy of binding of cations to aromatic groups ranges from 10 to 40 kcal/mol which places the cation−π interaction among the strongest noncovalent forces (*35*, *37*). The magnitude of the cation−π interaction depends on the geometry, distance, and nature of the cation and the aromatic group. In biological systems, the bulk of these interactions are seen with the amino acid side chains of proteins. Aromatic amino acids such as tryptophan, tyrosine, and phenylalanine interact with positively charged amino acids such as lysine and arginine. The energetics of these interactions have been

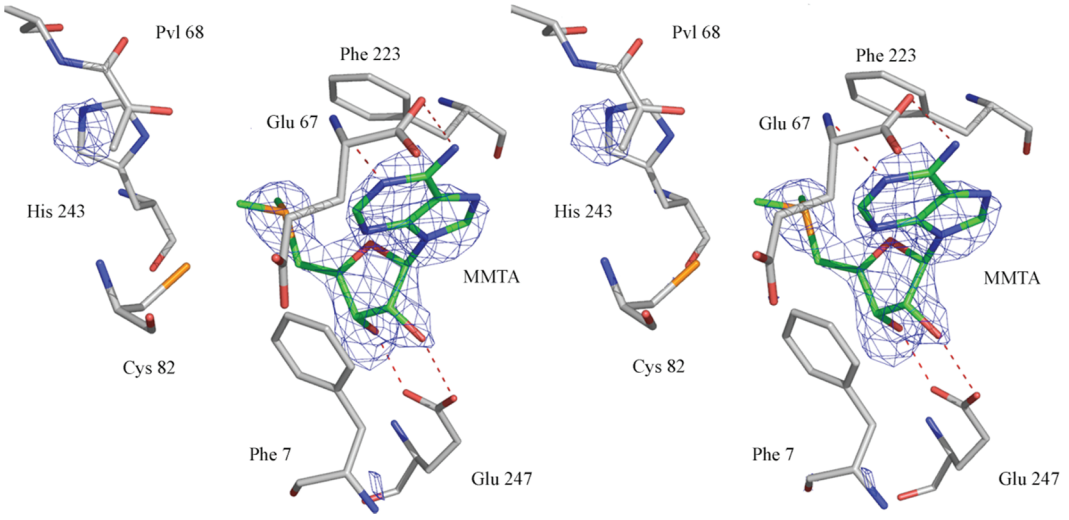

FIGURE 1: Stereoview of the complex of MMTA with AdoMetDC. The difference $F_o - F_c$ Fourier density is contoured at 2.5σ. The carbon atoms of the ligand are colored green. The hydrogen bonds are shown as red dashed lines.

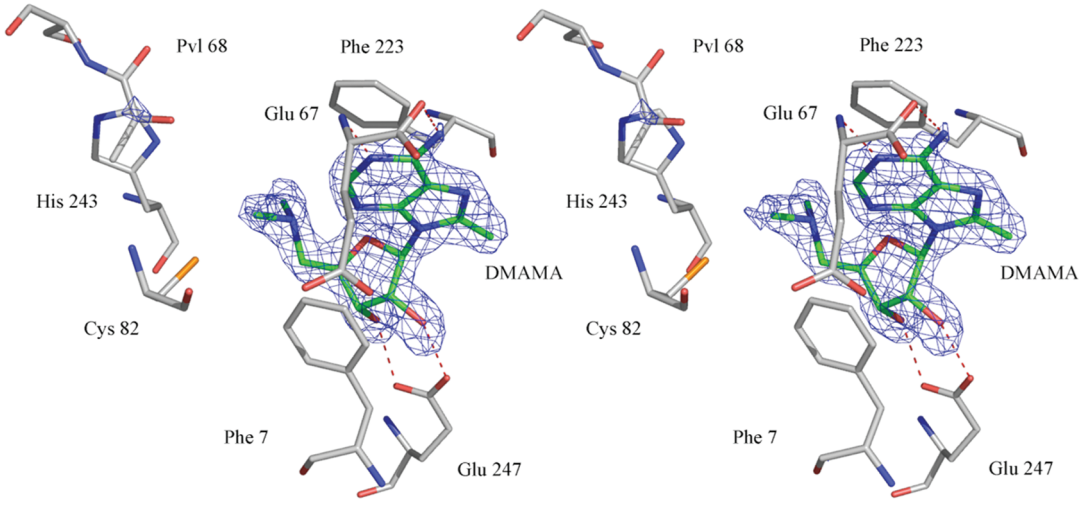

FIGURE 2: Stereoview of the complex of DMAMA with AdoMetDC. The difference $F_o - F_c$ Fourier density is contoured at 4σ. The carbon atoms of the ligand are colored green. The hydrogen bonds are shown as red dashed lines.

Table 3: Quantum Chemical Energies of Residues and Ligands

	energy (hartrees)
benzene	−231.47989407141
$(CH_3)_2S$	−477.13908367149
$(CH_3)_2S$, Phe223, and Phe7	−940.10191861550
$(CH_3)_3S^+$ and Phe223	−748.08525375049
$(CH_3)_3S^+$ and Phe7	−748.08567703979
$(CH_3)_3S^+$	−516.60034059742
$(CH_3)_3S^+$, Phe223, and Phe7	−979.57032658617

studied both experimentally and theoretically (*38*, *39*). In a few cases, ligand recognition by an enzyme is attributed completely to the cation−π interaction (*40*).

It has been shown that AdoMetDC binds substrate analogues only if they have a positive charge at the sulfonium position (*20*). MHZPA and MAOEA, which do not contain a sulfonium center, have an ammonium group that is protonated at physiological pH. The inability to form MTA and SAH complexes in cocrystallization experiments is consistent with this observation.

The results reported here suggest that cation−π interactions play a primary role in determining substrate specificity. The crystal structure of AdoMetDC with MMTA shows that the sulfonium center is at a favorable distance and geometry for a cation−π interaction with Phe223. The positive charge of the sulfonium ion is distributed to the adjacent methyl and the methylene groups (Figure 4). The methylene group of MMTA is at a favorable distance and geometry for a cation−π interaction with Phe7. The quantum chemical calculations suggest the stabilization of a $(CH_3)_3S^+$ group in the active site is primarily due to its interaction with Phe223 and Phe7. Other ligands with a positive charge such as MHZPA, MAOEA, MeAdoMet, and DMAMA exhibit similar interactions with Phe223 and Phe7 (Figure 5). The magnitude of stabilization obtained due to the cation−π interaction is approximately −4.5 kcal/mol. The interaction may be weakened from its maximum value by distribution of positive charge to adjacent carbon and hydrogen atoms and because of nonideal geometry.

The cation−π interaction as a theme for sulfonium recognition was debated by Markham et al. on the basis of a survey of the crystal structures of AdoMet with various enzymes (*30*). The

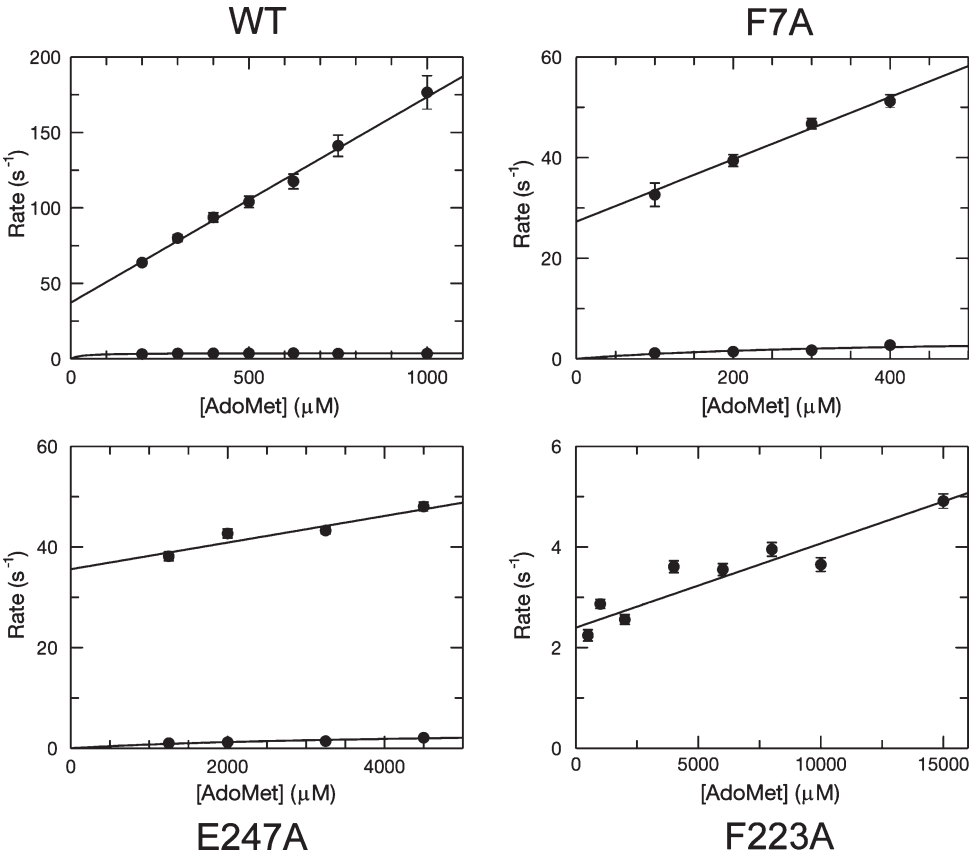

FIGURE 3: Plots of observed rates vs AdoMet concentration for the WT, F223A, F7A, and E247A enzymes. The linear concentration dependence of the observed rates was fit using a line which allowed for the definition of k_1 and k_{-1}. A hyperbolic fit of the slow phase defined the sum of k_2 and k_{-2}, except in the case of F223A, where the kinetics were monophasic and indicative of a more simple one-step binding model. In this case, the slope of the best fit line defines the k_1 and the y-intercept defines the k_{-1} directly.

survey which spanned 20 crystal structures showed that the sulfonium of AdoMet interacts with negatively charged atoms and aromatic amino acids in very few cases. In glycine-*N*-methyltransferase (PDB entry 1xva) and *Hha*I DNA methylase (PDB entry 1hmy), the sulfonium interacts with negatively charged carboxylate atoms (*41*, *42*). There are only two cases in the survey in which the sulfonium ion has a close contact with an aromatic group. The sulfonium ion of AdoMet is 3.2 Å from the methylene carbon atom of Trp41 in *Hha*I DNA methylase (PDB entry 1hmy), and in the structure of AdoMetDC with MeAdoMet bound (PDB entry 1i7b), the sulfonium ion is 4.1 Å from the center of Phe223. The survey concluded that in a broader picture, cation$-\pi$ interactions are not a recurring theme for sulfonium recognition. However, the uniqueness of the AdoMet decarboxylation reaction in this study may explain the importance of cation$-\pi$ interactions for AdoMetDC, which is further supported by theoretical calculations and stopped-flow kinetic experiments.

Stabilization of the syn Conformation by AdoMetDC. The conformational preference of AdoMet in solution and gas phase was studied by Markham et al. (*30*). According to the NMR studies, AdoMet prefers an *anti* conformation about the glycosidic bond in solution and a *syn* conformation in vacuum. The energy difference between the *anti* and *syn* conformations in solution was calculated to be −34 kcal/mol on the basis of the modeling studies using NMR constraints. This energy difference was calculated on the basis of molecular mechanics without polarization effects, and it is likely that the actual difference is less negative (*23*). The crystal structures of AdoMetDC with MeAdoMet, MHZPA, and MAOEA reported previously showed that the enzyme binds the ligands in the energetically unfavorable *syn* conformation (*22*).

The crystal structures of AdoMetDC with MMTA and DMAMA also show that the adenosine moiety binds in a *syn* conformation. The quantum chemical calculations for MMTA in a truncated model of the enzyme with only Phe7, Phe223, and Glu247 included suggest that the *syn* conformation of the ligand is stabilized by ~12 kcal/mol compared to the hypothetical *anti* conformation, which has never been observed in an AdoMetDC complex. The actual energy difference is likely to be greater than the value given above since the *anti* conformation places the six-membered ring of the adenine in the proximity of Asn224 and Pro225. Moreover, the amino group on the adenine ring is in the proximity of and forms hydrogen bonds to Glu67 in the *syn* conformation but forms no appreciable interactions with the enzyme in the *anti* conformation.

The *syn* conformation of the adenine base is primarily stabilized by stacking interactions with Phe7 and Phe223 and hydrogen bonds of the ribose to Glu247. N3 of the adenine base carries a partial negative charge and interacts favorably with the sulfonium ion. This electrostatic effect further contributes to the stabilization of the *syn* conformation of the ligand. The preference of AdoMetDC to bind ligands in the *syn* conformation was recently exploited in the design of substrate analogues with enhanced affinity. Substitution at the C^8 position on the adenine base favored the *syn* conformation, resulting in a 5−18-fold increase in potency compared to those of the unsubstituted compounds (*23*).

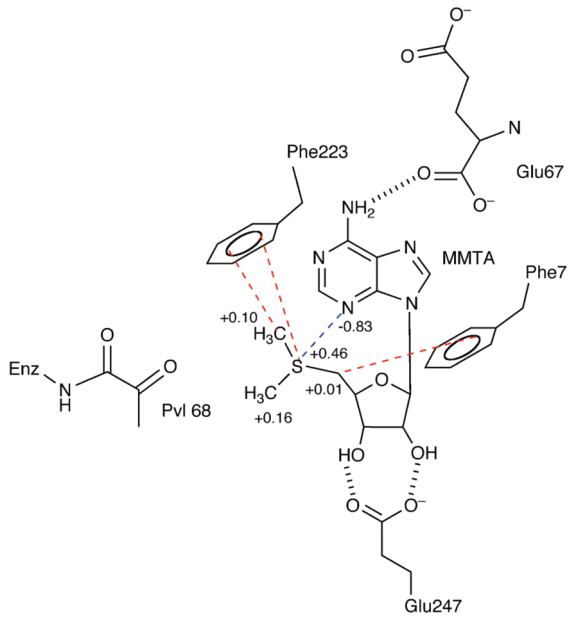

FIGURE 4: Schematic diagram of the key interactions MMTA makes in the active site of AdoMetDC. The adenine base stacks in the *syn* conformation aided by aromatic stacking interactions with Phe7 and Phe223. N6 of the adenine base forms a hydrogen bond to the backbone carbonyl of Glu67. The sulfonium ion and the terminal methyl group have a cation−π interaction with Phe223 (colored red), and the partially positively charged methylene group adjacent to sulfonium interacts with Phe7. N3 is partially negatively charged and interacts with the sulfonium. The partial charges on the relevant atoms are indicated. The ribose makes two hydrogen bonds to Glu247.

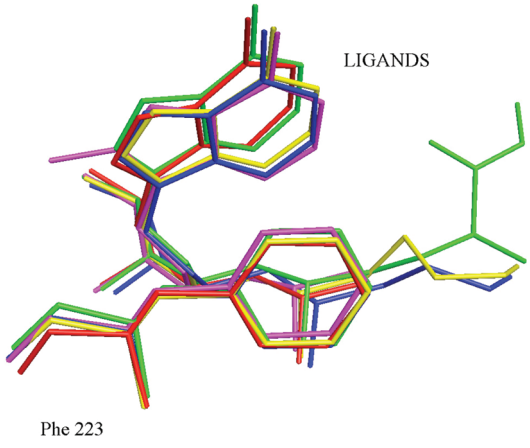

FIGURE 5: Superposition of the complexes of AdoMetDC showing the geometry of the cation−π interaction between the positive sulfonium/nitrogen and Phe223. The color coding for the complexes is as follows: red for MMTA, magenta for DMAMA, green for MeAdoMet, blue for MAOEA, and yellow for MHZPA.

Insights into Inhibitor Design. The design of substrate analogue inhibitors for AdoMetDC benefits from the presence of a positive charge required for the cation−π interaction. Unlike MAOEA and MHzPA, MMTA shows competitive inhibition because it lacks an amino terminus required to form a Schiff base with the active site pyruvoyl group. Studies on MMTA also show that the ribose, the adenine base, and the positive charge are sufficient for inhibition of AdoMetDC. The schematic diagram showing all of the stabilizing interactions of MMTA in the active site is shown in Figure 4.

The MMTA analogue DMAMA shows that the replacement of the sulfur with nitrogen also yields a competitive inhibitor because the nitrogen is protonated at physiological pH. DMAMA has a methyl substitution at the 8-position which should favor the *syn* conformation in solution and improve the binding to AdoMetDC (*23*). Because MMTA and DMAMA lack hydrazino or oxyamino groups, which react nonspecifically with cellular aldehydes and ketones, and because further evolution of their structures is possible, MMTA and DMAMA, with IC_{50} values of 15 μM and 600 nM (*23*), respectively, are promising lead compounds for inhibitor design.

ACKNOWLEDGMENT

We thank Ms. Leslie Kinsland for assistance in the preparation of the manuscript. We thank the Protein Production Facility, a Life Sciences Core Laboratory Center at Cornell University, for use of the stopped-flow apparatus. This work is based upon research conducted at beamlines 24-ID-C and 8-BM of the Northeastern Collaborative Access Team of the Advanced Photon Source, supported by Grant RR-15301 from the National Center for Research Resources at the National Institute of Health. Use of the Advanced Photon Source is supported by the U.S. Department of Energy, Office of Basic Energy Sciences, under Contract DE-AC02-06CH11357.

REFERENCES

(1) van Poelje, P. D., and Snell, E. E. (1990) Pyruvoyl-dependent enzymes. *Annu. Rev. Biochem. 59*, 29–59.
(2) Wallace, H. M., Fraser, A. V., and Hughes, A. (2003) A perspective of polyamine metabolism. *Biochem. J. 376*, 1–14.
(3) Casero, R. A.Jr., Celano, P., Ervin, S. J., Applegren, N. B., Wiest, L., and Pegg, A. E. (1991) Isolation and characterization of a cDNA clone that codes for human spermidine/spermine N^1-acetyltransferase. *J. Biol. Chem. 266*, 810–814.
(4) Gerner, E. W., and Meyskens, F. L.Jr. (2004) Polyamines and cancer: Old molecules, new understanding. *Nat. Rev. Cancer 4*, 781–792.
(5) Pegg, A. E., and Feith, D. J. (2007) Polyamines and neoplastic growth. *Biochem. Soc. Trans. 35*, 295–299.
(6) Hackert, M. L., and Pegg, A. E. (1997) Pyruvoyl-dependent enzymes. In Comprehensive Biological Catalysis (Sinnott, M. L., Ed.) pp 201−216, Academic Press, London.
(7) Pegg, A. E., Xiong, H., Feith, D., and Shantz, L. M. (1998) S-Adenosylmethionine decarboxylase: Structure, function and regulation by polyamines. *Biochem. Soc. Trans. 26* (580−586), 526.
(8) Tabor, C. W., and Tabor, H. (1984) Polyamines. *Annu. Rev. Biochem. 53*, 749–790.
(9) Tabor, C. W., and Tabor, H. (1984) Methionine adenosyltransferase (*S*-adenosylmethionine synthetase) and *S*-adenosylmethionine decarboxylase. *Adv. Enzymol. Relat. Areas Mol. Biol. 56*, 251–282.
(10) Williams-Ashman, H. G., and Schenone, A. (1972) Methylglyoxal bis(guanylhydrazone) as a potent inhibitor of mammalian and yeast *S*-adenosylmethionine decarboxylases. *Biochem. Biophys. Res. Commun. 46*, 288–295.
(11) Regenass, U., Mett, H., Stanek, J., Mueller, M., Kramer, D., and Porter, C. W. (1994) CGP 48664, a new *S*-adenosylmethionine decarboxylase inhibitor with broad spectrum antiproliferative and antitumor activity. *Cancer Res. 54*, 3210–3217.
(12) Eskens, F. A., Greim, G. A., van Zuylen, C., Wolff, I., Denis, L. J., Planting, A. S., Muskiet, F. A., Wanders, J., Barbet, N. C., Choi, L., Capdeville, R., Verweij, J., Hanauske, A. R., and Bruntsch, U. (2000) Phase I and pharmacological study of the weekly administration of the polyamine synthesis inhibitor SAM 486A (CGP 48 664) in patients with solid tumors. European Organization for Research and Treatment of Cancer Early Clinical Studies Group. *Clin. Cancer Res. 6*, 1736–1743.
(13) Zhou, H., Choi, L., Lau, H., Bruntsch, U., Vries, E. E., Eckhardt, G., Oosterom, A. T., Verweij, J., Schran, H., Barbet, N., Linnartz, R., and Capdeville, R. (2000) Population pharmacokinetics/toxicodynamics

(PK/TD) relationships of SAM486A in phase I studies in patients with advanced cancers. *J. Clin. Pharmacol. 40*, 275–283.
(14) Paridaens, R., Uges, D. R. A., Barbet, N., Choi, L., Seeghers, M., van der Graaf, W. T. A., and Groen, J. J. M. (2000) A phase I study of a new polyamine biosynthesis inhibitor, SAM486A, in cancer patients with solid tumours. *Br. J. Cancer 83*, 594–601.
(15) Siu, L. L., Rowinsky, E. K., Hammond, L. A., Weiss, G. R., Hidalgo, M., Clark, G. M., Moczygemba, J., Choi, L., Linnartz, R., Barbet, N. C., Sklenar, I. T., Capdeville, R., Gan, G., Porter, C. W., Von Hoff, D. D., and Eckhardt, S. G. (2002) A phase I and pharmacokinetic study of SAM486A, a novel polyamine biosynthesis inhibitor, administered on a daily-times-five every-three-week schedule in patients with advanced solid malignancies. *Clin. Cancer Res. 8*, 2157–2166.
(16) van Zuylen, L., Eskens, F., Bridgewater, J., Sparreboom, A., Sklenar, I., Planting, A., Choi, L., Mueller, C., Capdeville, R., Ledermann, J., and Verweij, J. (2000) The Polyamine Synthesis Inhibitor SAM486A in Combination, with 5-FU/LV in Metastatic Colorectal Cancer (MCC): Results of a Phase I and Pharmacokinetic Study. *Proc. Am. Soc. Clin. Oncol. 36*, 751.
(17) Pless, M., Belhadj, K., Kern, W., Dumontet, C., Chemnitz, J., Menssen, H. D., Herrmann, R., Barbet, N. C., and Capdeville, R. (2000) Clinical Efficacy of SAM486A, a Novel Polyamine Biosynthesis Inhibitor, in Patients with Refractory or Relapsed Non-Hodgkin's Lymphoma. *Proc. Am. Soc. Clin. Oncol. 36*, 62.
(18) Millward, M. J., Joshua, A., Kefford, R., Aamdal, S., Thomson, D., Hersey, P., Toner, G., and Lynch, K. (2005) Multi-centre Phase II trial of the polyamine synthesis inhibitor SAM486A (CGP48664) in patients with metastatic melanoma. *Invest. New Drugs 23*, 253–256.
(19) Shantz, L. M., Stanley, B. A., Secrist, J. A., and Pegg, A. E. (1992) Purification of human *S*-adenosylmethionine decarboxylase expressed in *Escherichia coli* and use of this protein to investigate the mechanism of inhibition by the irreversible inhibitors, 5′-deoxy-5′-[(3-hydrazinopropyl)methylamino]adenosine and 5′{[(Z)-4-amino-2-butenyl]methylamino}-5′-deoxyadenosine. *Biochemistry 31*, 6848–6855.
(20) Pankaskie, M., and Abdel-Monem, M. M. (1980) Inhibitors of polyamine biosynthesis 8: Irreversible inhibition of mammalian *S*-adenosyl-L-methionine decarboxylase by substrate analogs. *J. Med. Chem. 23*, 121–127.
(21) Pegg, A. E., and Jacobs, G. (1983) Comparison of inhibitors of S-adenosylmethionine decarboxylase from different species. *Biochem. J. 213*, 495–502.
(22) Tolbert, D. W., Ekstrom, J. L., Mathews, I. I., Secrist, J. A. I., Kapoor, P., Pegg, A. E., and Ealick, S. E. (2001) The structural basis for substrate specificity and inhibition of human *S*-adenosylmethionine decarboxylase. *Biochemistry 40*, 9484–9494.
(23) McCloskey, D. E., Bale, S., Secrist, J. A., Tiwari, A., Moss, T. H., Valiyaveettil, J., Brooks, W. H., Guida, W. C., Pegg, A. E., and Ealick, S. E. (2009) New Insights into the Design of Inhibitors of Human S-Adenosylmethionine Decarboxylase: Studies of Adenine C^8 Substitution in Structural Analogues of S-Adenosylmethionine. *J. Med. Chem. 52*, 1388–1407.
(24) Otwinowski, Z., and Minor, W. (1997) Processing of X-ray diffraction data collected in oscillation mode. *Methods Enzymol. 276*, 307–326.
(25) Brunger, A. T., Adams, P. D., Clore, G. M., DeLano, W. L., Gros, P., Grosse-Kunstleve, R. W., Jiang, J. S., Kuszewski, J., Nilges, M., Pannu, N. S., Read, R. J., Rice, L. M., Simonson, T., and Warren, G. L. (1998) Crystallography & NMR system: A new software suite for macromolecular structure determination. *Acta Crystallogr. D54*, 905–921.
(26) Jones, T. A., Zou, J.-Y., Cowan, S. W., and Kjeldgaard, M. (1991) Improved methods for the building of protein models in electron density maps and the location of errors in these models. *Acta Crystallogr. A47*, 110–119.
(27) Emsley, P., and Cowtan, K. (2004) Coot: Model-building tools for molecular graphics. *Acta Crystallogr. D60*, 2126–2132.
(28) Kleywegt, G. J., and Jones, T. A. (1998) Databases in protein crystallography. *Acta Crystallogr. D54*, 1119–1131.
(29) Mecozzi, S., West, A. P., and Dougherty, D. A. (1996) Cation-π interactions in simple aromatics: Electrostatics provide a predictive tool. *J. Am. Chem. Soc. 118*, 2307–2308.
(30) Markham, G. D., Norrby, P. O., and Bock, C. W. (2002) *S*-Adenosylmethionine conformations in solution and in protein complexes: Conformational influences of the sulfonium group. *Biochemistry 41*, 7636–7646.
(31) DeLano, W. L. (2002) The PyMOL Molecular Graphics System , DeLano Scientific, San Carlos, CA.
(32) Ekstrom, J. E., Matthews, I. I., Stanley, B. A., Pegg, A. E., and Ealick, S. E. (1999) The crystal structure of human *S*-adenosylmethionine decarboxylase at 2.25 Å resolution reveals a novel fold. *Structure 7*, 583–595.
(33) Ekstrom, J. L., Tolbert, W. D., Xiong, H., Pegg, A. E., and Ealick, S. E. (2001) Structure of a human *S*-adenosylmethionine decarboxylase self-processing ester intermediate and mechanism of putrescine stimulation of processing as revealed by the H243A mutant. *Biochemistry 40*, 9495–9504.
(34) Johnson, K. A. (1986) Rapid kinetic analysis of mechanochemical adenosinetriphosphatases. *Methods Enzymol. 134*, 677–705.
(35) Ma, J. C., and Dougherty, D. A. (1997) The Cation-π Interaction. *Chem. Rev. 97*, 1303–1324.
(36) Gallivan, J. P., and Dougherty, D. A. (1999) Cation-π interactions in structural biology. *Proc. Natl. Acad. Sci. U.S.A. 96*, 9459–9464.
(37) Ruan, C., and Rodgers, M. T. (2004) Cation-π interactions: Structures and energetics of complexation of Na^+ and K^+ with the aromatic amino acids, phenylalanine, tyrosine, and tryptophan. *J. Am. Chem. Soc. 126*, 14600–14610.
(38) Biot, C., Buisine, E., Kwasigroch, J. M., Wintjens, R., and Rooman, M. (2002) Probing the energetic and structural role of amino acid/nucleobase cation-π interactions in protein-ligand complexes. *J. Biol. Chem. 277*, 40816–40822.
(39) Biot, C., Buisine, E., and Rooman, M. (2003) Free-energy calculations of protein-ligand cation-π and amino-π interactions: From vacuum to proteinlike environments. *J. Am. Chem. Soc. 125*, 13988–13994.
(40) Zacharias, N., and Dougherty, D. A. (2002) Cation-π interactions in ligand recognition and catalysis. *Trends Pharmacol. Sci. 23*, 281–287.
(41) Cheng, X., Kumar, S., Posfai, J., Pflugrath, J. W., and Roberts, R. J. (1993) Crystal structure of the HhaI DNA methyltransferase complexed with *S*-adenosyl-L-methionine. *Cell 74*, 299–307.
(42) Fu, Z., Hu, Y., Konishi, K., Takata, Y., Ogawa, H., Gomi, T., Fujioka, M., and Takusagawa, F. (1996) Crystal structure of glycine N-methyltransferase from rat liver. *Biochemistry 35*, 11985–11993.